

Modeling scale-up of particle coating by atomic layer deposition

Angel Yanguas-Gil¹ and Jeffrey W. Elam¹

Applied Materials Division, Argonne National Laboratory, Lemont, IL 60439 (USA)

(*Electronic mail: ayg@anl.gov)

(Dated: 26 August 2024)

Atomic layer deposition (ALD) is a promising technique to functionalize particle surfaces for energy applications including energy storage, catalysis, and decarbonization. In this work, we present a set of models of ALD particle coating to explore the transition from lab scale to manufacturing. Our models encompass the main particle coating manufacturing approaches including rotary bed, fluidized bed, and continuously vibrating reactors. These models provide key metrics, such as throughput and precursor utilization, required to evaluate the scalability of ALD manufacturing approaches and their feasibility in the context of energy applications. Our results show that designs that force the precursor to flow through fluidized particles transition faster to a transport-limited regime where throughput is maximized. They also exhibit higher precursor utilization. In the context of continuous processes, our models indicate that it is possible to achieve self-extinguishing processes with almost 100% precursor utilization. A comparison with past experimental results of ALD in fluidized bed reactors shows excellent qualitative and quantitative agreement.

I. INTRODUCTION

Over the past 20 years, there has been an increasing interest in the use of atomic layer deposition (ALD) for energy and decarbonization applications. Many of these approaches leverage the intrinsic conformality of ALD to functionalize or coat particles¹⁻³. Two examples are batteries⁴ and catalysis⁵: in battery research it has long been known that a few ALD cycles of materials such as Al₂O₃ on cathode particles improve device stability, preventing issues such as capacity fade⁶. In catalysis, ALD has been used to engineer catalyst supports^{7,8}, synthesize catalytic nanoparticles^{9,10}, and prevent catalyst degradation through protective overcoatings^{11,12}.

One of the perceived drawbacks of ALD is that it is a slow process: in addition to its pulsed, sequential nature – with each ALD cycle involving alternate exposures to two different precursors separated by purge times, in self-limited processes the reactivity of the surface goes down as the number of available reaction sites decreases. This typically reduces throughput compared to non self-limited processes like chemical vapor deposition (CVD).

Intuitively, we understand that as we scale an ALD process to larger batch sizes and increasingly higher surface areas, the process will eventually transition from a reaction limited regime to a transport limited regime, thereby eliminating some of the inefficiencies related to the self-limited surface kinetics. Currently, though, we do not have a good understanding of when and how the transition takes place, and how the underlying surface kinetics and the manufacturing approach affects this transition. This complicates the transfer of ALD processes from the lab to manufacturing.

In this work, we explore the fundamentals of the scale-up of particle coating by ALD. In particular, we focus on three common manufacturing approaches for particle coating: rotating drum^{13,14}, fluidized bed¹⁵, and continuous reactors^{16,17}, generalizing traditional chemical engineering models to incorporate the spatial and time dependencies intrinsic to self-limited processes¹⁸. In a prior work, we showed how this approach provided excellent qualitative and quantitative agreement for the specific case of a fluidized bed reactor¹⁹. There is there-

fore an opportunity to apply the same methodology to other scaling approaches and to expand the range of surface kinetics models considered.

II. MODEL

A. Surface kinetics

1. Ideal self-limited model

A key feature of self-limited processes is the presence of a finite number of reactive sites on the surface. Using the open site formalism²⁰, the surface reactivity can be represented by a sticking probability, β , that depends on the fraction of surface sites available for precursor molecules to react with at a given time. If we define the fractional coverage, Θ , as the fraction of surface sites that have already reacted, the simplest model introduces a first-order dependence on the fraction of available sites, $1 - \Theta$:

$$\beta = \beta_0(1 - \Theta) \quad (1)$$

Where β_0 represents the reaction probability of the precursor molecule with an available site. This model, which corresponds to a first order irreversible Langmuir kinetics, is one of the most commonly used in the literature to model the surface kinetics of an ALD process²¹⁻²⁴.

The evolution of the fractional surface coverage is therefore given by:

$$\frac{d\Theta}{dt} = s_0\beta_0(1 - \Theta)J \quad (2)$$

where s_0 represent the average surface area of a reactive site, and J represents the surface flux of precursor molecules (number of precursor molecules reaching the surface per unit area and unit time), which can be calculated from the precursor partial pressure, p , and the process temperature, T :

$$J = \frac{1}{4}v_{th}n = \frac{1}{4}v_{th}\frac{p}{k_B T} \quad (3)$$

Here v_{th} is the precursor thermal velocity, n is the precursor molecular density (number of molecules per unit volume), and k_B is Boltzmann's constant.

2. Extension to heterogeneous surfaces

The model above represents the ideal case where the surface can be partitioned into identical reaction sites. However, in many cases of interest surfaces are heterogeneous, which means that we need to extend Eq. 1 to consider the presence of multiple sites:

$$\beta = \sum_s f_s \beta_s (1 - \Theta^s) \quad (4)$$

With f_s representing the fraction of each site, β_s is the reaction probability of the precursor molecule with that site, and $\sum_s f_s \leq 1$ is the total fraction of reactive surface sites. There are two cases of interest for this work: the first is when only a fraction of the surface is reactive towards the ALD precursor. In this case, if f represents the fraction of the sites that are reactive, we have that:

$$\beta = f \beta_0 (1 - \Theta) \quad (5)$$

resulting in a lower sticking probability, with the evolution of Θ still given by Eq. 2. This case is representative of surface functionalization or passivation approaches where nucleation is potentially sparse. Including f in our model allows us to independently tune the size of a surface site, given by its area s_0 , and the number of active sites on the surface. The second case comprises surfaces with two types of reactive sites, one with high and another one with low sticking probability²⁵. This scenario allows us to consider ‘‘soft-saturating’’ ALD processes, where after an initially fast mass uptake, the growth per cycle as a function of dose time asymptotically reaches a limiting value²⁴. In this scenario, the sticking probability is given by:

$$\beta = f_a \beta_a (1 - \Theta_a) + f_b \beta_b (1 - \Theta_b) \quad (6)$$

Where Θ_a and Θ_b are the fractional coverage of sites a and b, f_a and f_b are the fraction of sites for each reaction pathways, and the total fractional surface coverage is given by:

$$\Theta = f_a \Theta_a + f_b \Theta_b \quad (7)$$

In this case, both Θ_a and Θ_b evolve as a function of time following Eq. 2.

B. Reactor models

In this work we introduce models for two batch and two continuous ALD particle coating strategies (Table I). For the batch cases, which correspond to rotating drum and fluidized bed reactors, we assume homogeneous particle mixing, whereas for the continuous processes we assume that mixing takes place preferentially in the directions perpendicular to

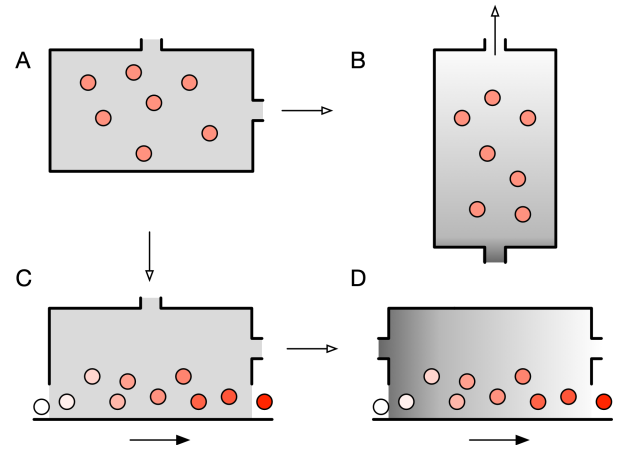


FIG. 1. Four type of reactor models considered in this work: A) well-mixed batch process; B) plug flow batch process; C) well-mixed continuous process; D) plug flow continuous process. In these diagrams, the white arrows show the direction of precursor flow, and the black arrows designate the direction of particle transport. The particle shading represents the degree of saturation with dark red indicating complete coverage. The background shading indicates precursor concentration with darker shading representing a higher concentration.

particle transport^{17,26}. Examples of continuous processing include continuous vibrating reactors (CVR). A second key assumption involves how precursor delivery takes place in these reactors: the well-mixed approximation is a valid assumption when the geometry of the reactor favors mixing and mixing takes place faster than the characteristic dose time [Fig. 1(A)]. Alternatively, the reactor can be designed to force precursor to flow through the agitated particles. For fluidized bed ALD reactors, in a prior work we showed that a plug flow model of precursor transport reproduced well reactor configurations where precursor is introduced upstream of the reactor and is delivered by the same flow used for particle fluidization¹⁹ [Fig. 1(B)]. Finally, for the continuous fluidized bed we consider both the well-mixed and cross-flow cases, which would correspond to short and long reactor geometries [Figs. 1(C) and 1(D), respectively]. The mapping between these models and strategies for particle coatings is not one-to-one: for instance, fluidized bed reactors can be designed to operate in batch or continuous mode; rotating drum reactors can have geometries that favor mixing or that transport the precursor along the axis of revolution. Some of the possible combinations are enumerated in Table I.

These four models share a series of common parameters, including the reactor volume, V , total surface area to be coated, S , and the precursor residence time, t_{res} . Also, n_0 and p_0 are the precursor molecular density and pressure at the inlet, respectively. Models that explicitly consider either particle or gas transport in the reactor depend on the reactor length, L , its cross-sectional area, S_0 , the flow velocity, u , and the particle velocity, v .

TABLE I. Summary of models and conditions explored in this work

Model	Process type	Particle mixing	Precursor transport	Examples
A	Batch	Homogeneous	Well-mixed	Rotating drum
B	Batch	Homogeneous	Plug flow	Fluidized bed, rotating drum
C	Continuous	In plane mixing	Well-mixed	CVR, spatial ALD
D	Continuous	In plane mixing	Plug flow	CVR, fluidized bed, spatial ALD

1. Batch process with well-mixed reactor approximation

This model assumes ideal mixing so that all particles are homogeneously coated [Figure 1(A)]. Furthermore, the precursor is also efficiently mixed in the reactor, so that the well-mixed approximation applies. An example would be a rotating drum reactor under near-static precursor flow conditions.

For a single reactive pathway, the model equations are:

$$\frac{V}{t_{\text{res}}}(n_0 - n) = Sf\beta_0(1 - \Theta)\frac{1}{4}v_{th}n \quad (8)$$

$$\frac{d\Theta}{dt} = s_0\beta_0(1 - \Theta)\frac{1}{4}v_{th}n \quad (9)$$

Whereas for a soft-saturating system the model equations are:

$$\frac{V}{t_{\text{res}}}(n_0 - n) = S[(1 - f)\beta_a(1 - \Theta_a) + f\beta_b(1 - \Theta_b)]\frac{1}{4}v_{th}n \quad (10)$$

$$\frac{d\Theta_a}{dt} = s_0\beta_a(1 - \Theta_a)\frac{1}{4}v_{th}n \quad (11)$$

$$\frac{d\Theta_b}{dt} = s_0\beta_b(1 - \Theta_b)\frac{1}{4}v_{th}n \quad (12)$$

This model is representative of particle coating approaches such as rotating drum reactors.

2. Batch process with plug flow precursor transport

We next consider a plug flow model for the precursor transport across a homogeneously mixed particle column of cross section area S_0 and length L [Figure 1(B)]. Examples for this type of reactor include a fluidized bed or a rotating drum under cross-flow conditions. In this case, the precursor balance is given by:

$$S_0u\frac{dn}{dz} = -\frac{S}{L}f\beta(t)\frac{1}{4}v_{th}n \quad (13)$$

where u is the flow velocity. This leads to the following equations for the single reaction pathway case:

$$S_0u\frac{dn}{dz} = -\frac{S}{L}f\beta_0(1 - \Theta)\frac{1}{4}v_{th}n \quad (14)$$

$$\frac{d\Theta}{dt} = s_0\beta_0(1 - \Theta)\frac{1}{4}v_{th}\bar{n} \quad (15)$$

$$\bar{n} = \frac{1}{L}\int_0^L n(z)dz \quad (16)$$

where \bar{n} is the average precursor density along the column.

The following equations are obtained for the soft-saturating ALD case:

$$S_0u\frac{dn}{dz} = -\frac{S}{L}[(1 - f)\beta_a(1 - \Theta_a) + f\beta_b(1 - \Theta_b)]\frac{1}{4}v_{th}n \quad (17)$$

$$\frac{d\Theta_a}{dt} = s_0\beta_a(1 - \Theta_a)\frac{1}{4}v_{th}\bar{n} \quad (18)$$

$$\frac{d\Theta_b}{dt} = s_0\beta_b(1 - \Theta_b)\frac{1}{4}v_{th}\bar{n} \quad (19)$$

3. Continuous process and well-mixed precursor approximation

We next consider particles moving with a velocity v inside a reactor of length L [Figure 1(C)]. The particles are only partially mixed, with perfect mixing only in the plane perpendicular to the direction of movement of the particles. Consequently, the surface coverage depends only on the particle position along the upstream-downstream axis: $\Theta = \Theta(z)$ and on the total exposure received until reaching z . Furthermore, the well-mixed approximation holds for the ALD precursor transport. An example for this type of system would be a vibro-fluidized bed reactor under near static flow conditions. For a single heterogeneous process, the model equations are:

$$\frac{V}{t_{\text{res}}}(n_0 - n) = Sf\beta_0(1 - \bar{\Theta})\frac{1}{4}v_{th}n \quad (20)$$

$$v\frac{d\Theta}{dz} = s_0\beta_0(1 - \Theta)\frac{1}{4}v_{th}n \quad (21)$$

Where $\bar{\Theta}$ is the average reactivity along the upstream downstream axis:

$$\bar{\Theta} = \frac{1}{L}\int_0^L \Theta(z)dz \quad (22)$$

This model is trivially extended to the soft-saturating case:

$$\frac{V}{t_{\text{res}}}(n_0 - n) = S[(1 - f)\beta_a(1 - \bar{\Theta}_a) + f\beta_b(1 - \bar{\Theta}_b)]\frac{1}{4}v_{th}n \quad (23)$$

and

$$v\frac{d\Theta_a}{dz} = s_0\beta_a(1 - \Theta_a)\frac{1}{4}v_{th}n \quad (24)$$

$$v\frac{d\Theta_b}{dz} = s_0\beta_b(1 - \Theta_b)\frac{1}{4}v_{th}n \quad (25)$$

with:

$$\bar{\Theta}_a = \frac{1}{L} \int_0^L \Theta_a(z) dz \quad (26)$$

$$\bar{\Theta}_b = \frac{1}{L} \int_0^L \Theta_b(z) dz \quad (27)$$

4. Continuous process with plug flow precursor transport

The final model considers the case of a continuous process in which the precursor is injected in an upstream position and flows downstream over a fluidized bed of particles moving in the same direction [Figure 1(D)]. In this case, both the fractional surface coverage and the precursor concentration depend on the axial position. For the case of a single heterogeneous process:

$$S_0 u \frac{du}{dz} = -\frac{S}{L} f \beta_0 (1 - \Theta) \frac{1}{4} v_{th} n \quad (28)$$

$$v \frac{d\Theta}{dz} = s_0 \beta_0 (1 - \Theta) \frac{1}{4} v_{th} n \quad (29)$$

which again can be trivially extended to the soft-saturating case:

$$S_0 u \frac{dn}{dz} = -\frac{S}{L} [(1-f)\beta_a(1-\Theta_a) + f\beta_b(1-\Theta_b)] \frac{1}{4} v_{th} n \quad (30)$$

$$v \frac{d\Theta_a}{dz} = s_0 \beta_a (1 - \Theta_a) \frac{1}{4} v_{th} n \quad (31)$$

$$v \frac{d\Theta_b}{dz} = s_0 \beta_b (1 - \Theta_b) \frac{1}{4} v_{th} n \quad (32)$$

C. Model normalization

In order to establish a comparison between these models we will use two common non-dimensional numbers: the first is the Damköhler number, which can be defined as the ratio of the characteristic reaction rate and the transport rate:

$$Da = \frac{\text{reaction rate}}{\text{transport rate}} \quad (33)$$

For the case of a single heterogeneous process, we define the Damköhler number as:

$$Da = \frac{S}{V} \beta_0 \frac{1}{4} v_{th} t_{res} \quad (34)$$

In the case of plug-flow models, the residence time is defined as $t_{res} = L/u$. We can introduce the case of sparse nucleation ($f < 1$) by defining an effective surface area $S_{eff} = fS$. For the soft-saturating case, we can define a Damköhler number for each surface reaction pathway, Da_i .

The second non-dimensional number is a characteristic time that depends on the precursor residence time and the

number of precursor molecules in the reactor per surface site, which in the context of the ALD has been referred to as the excess number, γ :

$$t_0 = t_{res} \frac{S}{s_0 n_0 V} = \frac{t_{res}}{\gamma} \quad (35)$$

For a batch process, we can define a normalized dose time in terms of t_0 :

$$\tau = \frac{t}{t_0} \quad (36)$$

The meaning of τ is that $\tau = 1$ corresponds to the time at which the total number of precursor molecules inserted in the reactor is equal to the total number of reactive sites.

For a continuous process, we define a normalized particle residence time:

$$\tau_s = \frac{t_s}{t_0} \quad (37)$$

where t_s is the average particle residence time inside the reactor $t_s = L/v$. As before, $\tau_s = 1$ corresponds to the point at which precursor molecules and surface sites are introduced at equal rates.

Finally, we define a normalized reactor length, $\xi = z/L$, and a normalized precursor concentration, $x = n/n_0$.

The resulting non-dimensional equations for the four models in both the single heterogeneous process case and the soft-saturation case are provided in the Supporting Information.

III. RESULTS

A. Model solutions

The four models introduced above can be solved exactly for the case of a single reaction pathway described by Eq. 5.

For a batch process, the fractional coverage Θ of the well-mixed and plug flow models are given in terms of the normalized dose time τ and the Damköhler number, Da , by:

$$\tau = \Theta - \frac{1}{Da} \log(1 - \Theta) \quad (38)$$

and

$$\Theta = 1 - \frac{1}{Da} \log(1 + (e^{Da} - 1)e^{-Da\tau}) \quad (39)$$

respectively.

Interestingly, the expression for the final surface coverage for the continuous well-mixed process is identical to the batch well-mixed process case (Eq. 38), except that it depends on the normalized residence time τ_s instead:

$$\tau_s = \Theta - \frac{1}{Da} \log(1 - \Theta) \quad (40)$$

Finally, the surface coverage for the continuous plug flow model is given by:

$$\Theta = 1 - \frac{1 - \tau_s}{1 - \tau_s e^{-(1 - \tau_s)Da}} \quad (41)$$

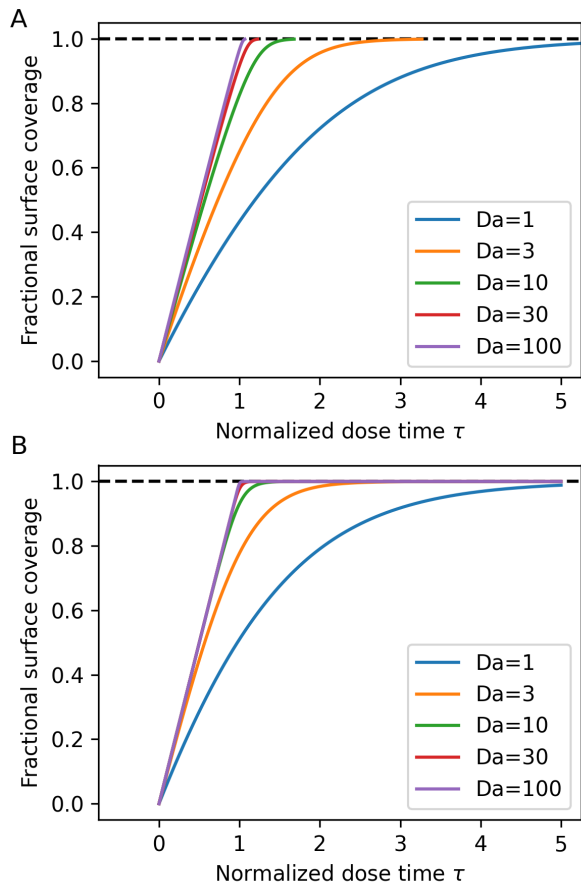


FIG. 2. Saturation curves showing the fractional surface coverage of particles as a function of the normalized dose time for the (A) well-mixed batch and (B) plug flow batch models. As the Damköhler number increases, both processes transition from a reaction limited to a transport limited regime.

B. Scale up of batch processes

The value of Da increases with increasing amount of surface area inside the reactor. Consequently, it is a useful parameter that can be applied to track the behavior of a process upon scale up. An ideal process would achieve saturation in the minimum possible time and utilize 100% of the supplied precursor. As will be shown below, all of the reactor models approach ideal behavior in the limit of high Da , but the degree of ideality varies among the models and this highlights differences in their scalability.

Figure 2 shows saturation plots with the evolution of the fractional surface coverage as a function of dose time for batch processes with the well-mixed [Fig 2(A)] and plug flow [Fig 2(B)] precursor transport approximations. Results are shown for increasing values of the Damköhler number.

The plots are represented using the normalized dose time τ . A value of $\tau = 1$ represents the time at which the total number of moles of precursor inserted in the reactor equals the total number of surface reactive sites, so a fractional surface coverage approaching one for $\tau = 1$ indicates that the process is

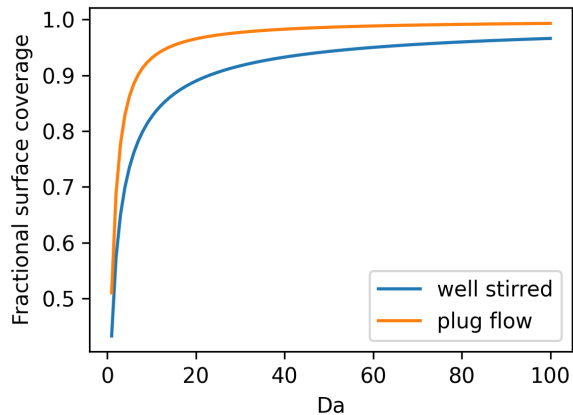


FIG. 3. Fractional surface coverage of particles coated by ALD in a batch process for a normalized dose time $\tau = 1$ as a function of the Damköhler number. Reactors whose precursor transport can be approximated by a plug flow model transition faster from a reaction limited to a transport limited regime compared to the well-mixed model, characterized by a saturation time equal to $\tau = 1$.

reaching the transport-limited regime and approaching ideal behavior. For both the well-mixed and plug flow models, the slope of fractional coverage vs dose time increases with increasing values of Da . The time to saturation also shortens, reaching values close to $\tau = 1$, thus confirming that ALD processes do become more efficient as they are scaled. However, that transition takes place at lower Damköhler numbers for the plug flow model, with the transition taking place for $Da > 10$, whereas for the well-mixed reactor the transition requires $Da > 30$.

One way of visualizing the transition from a reaction to a transport-limited regime is by tracking the fractional surface coverage for $\tau = 1$ as a function of the Damköhler number. This is shown in Figure 3 for both the well-mixed and plug flow models. The results show that the plug flow model transitions faster to a reaction limited regime, achieving larger fractional surface coverages than the well-mixed model for the same process and surface area (equal Da).

A crucial metric for manufacturing is precursor efficiency, which we define as the percentage of precursor molecules that are used in the deposition process. In Figure 4 we show the precursor efficiency for both the well-mixed and plug flow models as a function of the final fractional surface coverage for increasing values of the Damköhler number. At low Damköhler numbers, the precursor utilization is low due to the intrinsic slow down of the surface kinetics in self-limited processes. However, as the Damköhler number increases, the process becomes increasingly more efficient until reaching almost 100% precursor utilization. As shown above for the fractional surface coverage, the plug flow model yields a higher precursor efficiency than the well-mixed model for identical fractional surface coverage and Damköhler number.

Likewise, in Figure 5 we show the fraction of unreacted precursor that leaves the reactor as a function of normalized dose time for both batch processes. This depiction of precursor effi-

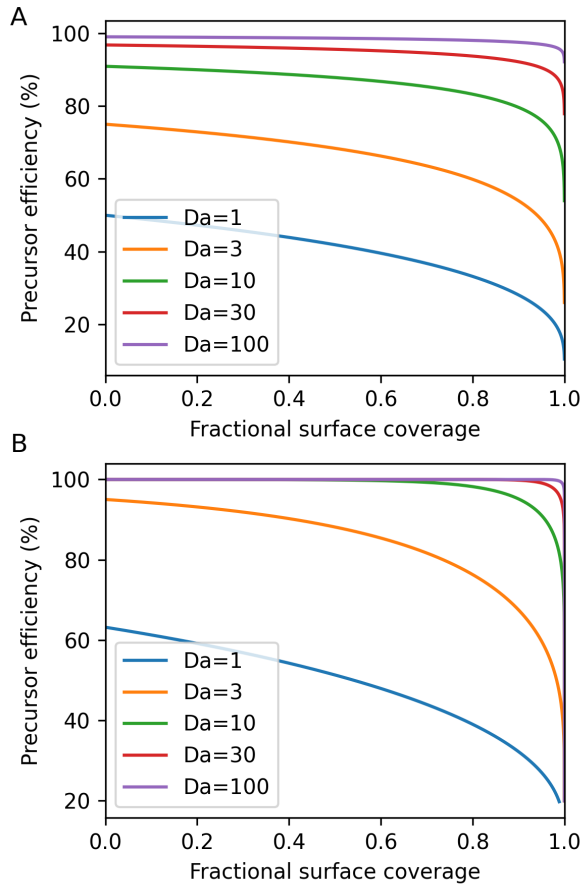


FIG. 4. Fraction of precursor used for coating particles as a function of the final target fractional surface coverage for (A) a well-mixed batch and (B) a plug flow batch process. Both processes become more efficient with increasing Damköhler number, with the plug flow batch process outperforming the well-mixed batch process.

ciency is useful because it models a downstream measurement of the precursor concentration using a mass spectrometer. The high precursor efficiencies shown in Figure 4 consistently lead to almost no precursor leaving the reactor prior to reaching saturation. However, as the system transitions to a transport limited regime, the “punch-through” signal of unreacted precursor becomes increasingly more sharp at the point where saturation is reached. This agrees well with experimental observations showing how in-situ mass spectrometry provides a characteristic punch-through signal for particle coated by a TMA/H₂O ALD process in a fluidized bed reactor^{2,19}.

C. Scale up of continuous processes

Continuous processes differ from batch processes in two ways: first, in a continuous process the precursor is constantly dosed into the reactor volume so that the residence time of the particles inside the reactor, t_s , and the corresponding normalized residence time, τ_s (Eq. 37), determine the total exposure. Second, the fractional surface coverage of the particles

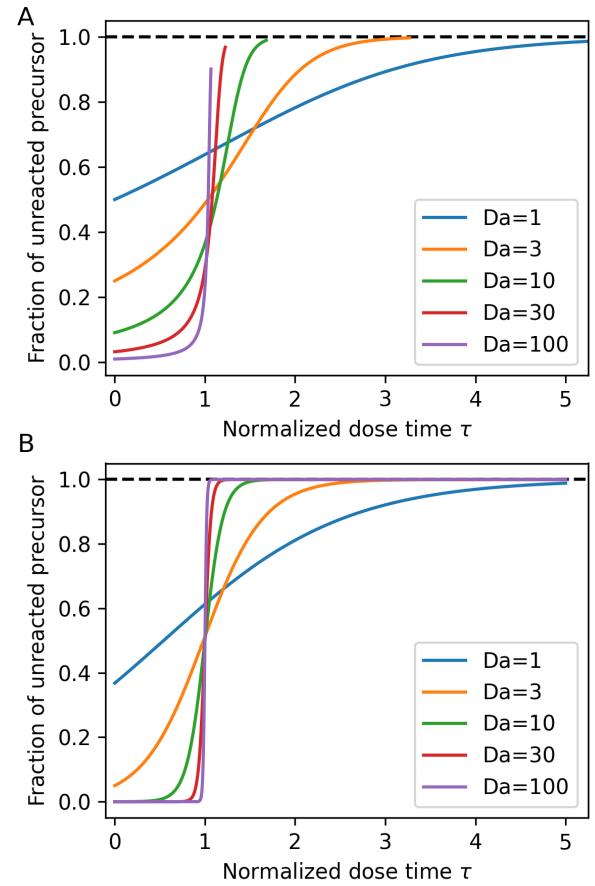


FIG. 5. Fraction of unreacted precursor for the (A) well-mixed batch and (B) plug flow batch models as a function of normalized dose time and increasing Damköhler numbers. Under the precursor transport limited regime, a clear signature from the precursor is observed as the ALD process reaches saturation.

increases as particles move inside the reactor. A key metric for evaluating the manufacturability of continuous processes is therefore the fractional coverage as the particles exit the reactor.

As mentioned in Section III A, in the case of an ideal self-limited process, the solution for the continuous well-mixed model is identical to that of the well-mixed batch model, except that the dose time, τ , is replaced with the normalized particle residence time, τ_s (Eq. 40). The results shown in Figures 2(A) and 4(A) are therefore applicable to the well-mixed continuous model.

The key features of the plug flow continuous model are shown in Figure 6. In Figure 6(A) we show saturation curves for increasing Damköhler numbers as a function of the normalized particle residence time, τ_s . Here the particle residence time can be viewed as the inverse of the rate or velocity at which particles are being fed into the reactor. As in the case of batch processes, achieving saturation at $\tau_s = 1$ indicates a transition to the transport-limited regime. In Figure 6(B) we show the fraction of unreacted precursor for the same parameters used in Figure 6(A). In the limit of very high rates

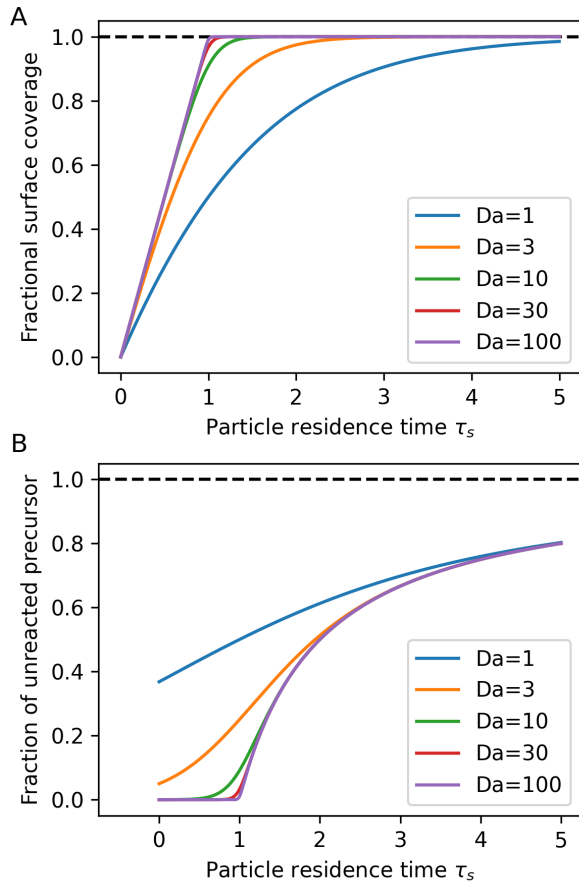


FIG. 6. (A) Saturation curves showing the fractional surface coverage of particles as a function of the normalized particle residence time and increasing Damköhler numbers for a continuous plug flow model for particle coatings by ALD. (B) Fraction of unreacted precursor for the same conditions.

of particle insertion ($\tau_s \rightarrow 0$), particles move so fast that the precursor reacts with a fully reactive surface. Therefore, the precursor utilization is the highest at very low residence times. High Damköhler numbers lead to almost 100% precursor utilization in this regime. As the residence time increases, the surface coverage of the particles exiting the reactor increases. For high Damköhler numbers, there is a clear transition for $\tau_s = 1$, when particles leave the reactor fully saturated and the fraction of unreacted precursor starts to increase. Consequently, like in the batch plug flow models, there is a clear signature indicating the optimal particle insertion rate at which saturation is achieved. However, this transition is less abrupt than in batch processes (Fig. 5), since in a continuous process particles are constantly being fed into the reactor and therefore there is still a significant amount of precursor used after reaching saturation.

In Figure 7 we compare the fractional surface coverage achieved at $\tau_s = 1$ in the well-mixed and plug flow continuous models. As in the case of batch processes, the plug flow model consistently leads to higher fractional surface coverages across the whole range of Da explored. This highlights

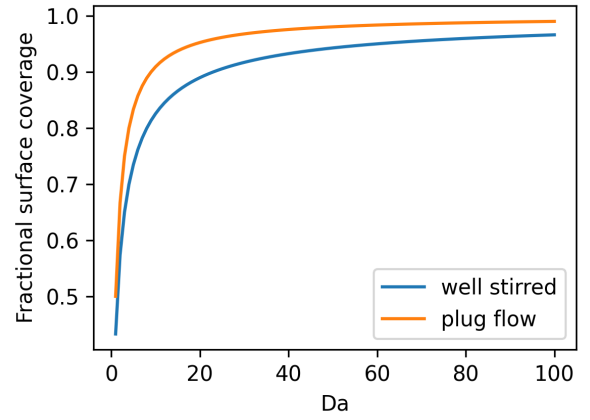


FIG. 7. Fractional surface coverage of particles coated by ALD in a continuous process for a normalized particle residence time $\tau_s = 1$ as a function of the Damköhler number. As in the case of batch processes, reactors whose precursor transport can be approximated by a plug flow model are more efficient.

the importance of reactor design and precursor delivery to ensure a faster transition to a transport limited regime and an optimal precursor utilization.

D. Extension to soft-saturating processes

The results obtained thus far have focused on an ideal irreversible first order Langmuir surface kinetics. When we extend the models to the soft-saturating case, we observe similar trends, with the plug-flow approximation being consistently faster in transitioning to a transport limited regime and achieving high precursor utilization than the well-mixed approximation for both continuous and batch processes.

As an example of a soft-saturating process, we have considered a system where the second pathway is ten times less reactive than the main reaction pathway. Based on Eq. 34, this means that $Da_2 = 0.1 \times Da_1$. In Figure 8, we show the saturation profiles for increasing values of Da_1 for the well-mixed batch process. The presence of a second, slower reaction pathway softens the transition from reaction limited to transport limited regime, with the soft saturating component pushing the transition to higher values of Da_1 due to the presence of the secondary reaction pathway with a lower reactivity. The behavior observed for this model is representative of the plug flow and continuous models.

IV. DISCUSSION

The four models introduced in this work allow us to evaluate the scalability of different strategies for particle coatings by atomic layer deposition by calculating the transition from reaction-limited to transport limited regimes. In all cases, this transition is dictated by the Damköhler number (Eq. 34). In

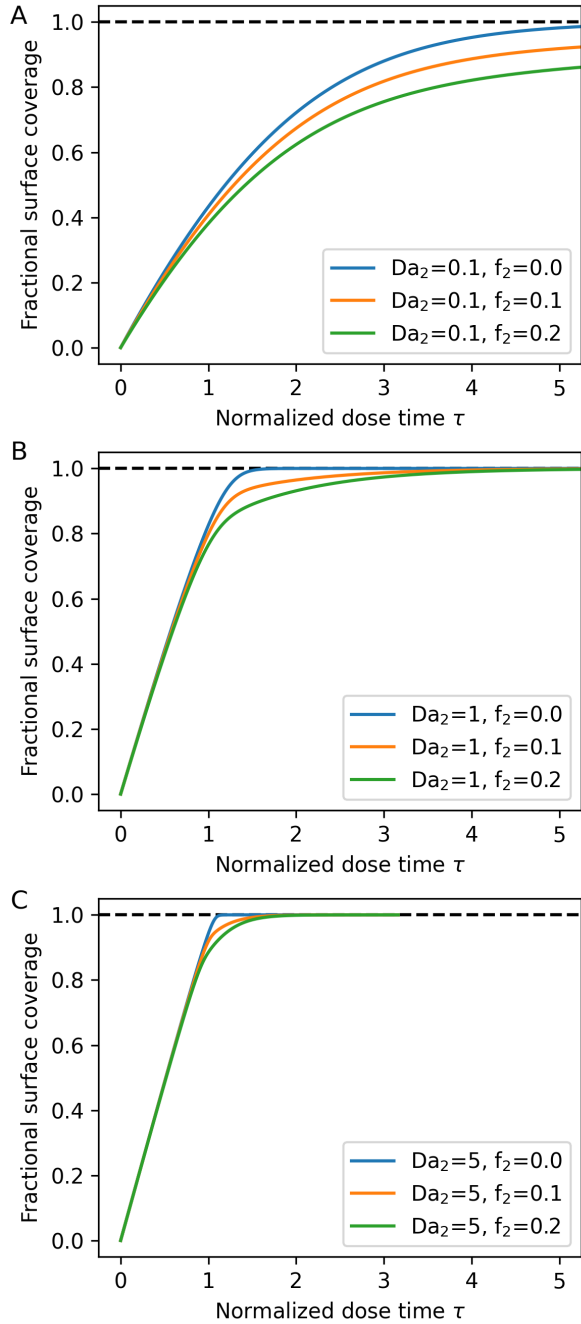


FIG. 8. Saturation curves in a well-mixed batch process for a soft-saturating ALD process. Results are shown for increasing values of the Damköhler number of the main surface reaction pathway: (A) $Da_1 = 1$; (B) $Da_1 = 10$; (C) $Da_1 = 50$. In all cases, $Da_2 = 0.1 \times Da_1$.

terms of the volumetric flow ϕ (in m^3s^{-1}) into the reactor, the Damköhler number is given by:

$$Da = \frac{S}{\phi} \beta_0 \frac{1}{4} v_{th} \quad (42)$$

Here, all the parameters except for the sticking probability, β_0 , and the fraction of reactive sites f are available experimen-

tally: the mean thermal velocity, v_{th} , depends on the precursor molecular mass and process temperature, the volumetric flow, ϕ , can be calculated from the process pressure and the standard flow in the mass flow controllers, and S is the total surface area of the particles inside the reactor. If only a fraction f of the sites are reactive, this effect can be incorporated as an effective surface $S_{\text{eff}} = fS$.

In the transport limited regime, the saturation dose time or the particle residence time is given simply by the time required to introduce into the reactor a number of precursor molecules equal to the number of available surface sites. This will be limited by the maximum precursor partial pressure that can be delivered at a volumetric flow, ϕ . It also depends on the number of surface sites per unit area, which can be extracted from the growth per cycle of the ALD process. Consequently, if we assume that $f = 1$, the sticking probability is the only parameter that is generally not known in an ALD process.

The results obtained also emphasize the importance of reactor design in ensuring a fast and efficient transition from a reaction-limited to a transport-limited regime: the plug flow model consistently leads to faster processes and higher precursor utilization in both batch and continuous ALD configurations. In the batch process case, fluidized bed reactors are one way of achieving this cross flow: indeed, in a prior work we showed good qualitative and quantitative agreement between the plug flow model and experimental results of particle coating by TMA/water¹⁹. In the continuous case, plug flow configurations show additional properties, such as a self-extinguishing behavior: as shown in Figure 6, the process conditions can be optimized to achieve saturation while minimizing the fraction of unreacted precursor. This can prove beneficial in spatial ALD configurations where isolation between different precursor zones is key.

Finally, the presence of soft-saturating processes shifts the transition to a transport limited regime to higher Damköhler numbers of the leading, more reactive process due to the need to accommodate slower reaction pathways. However, as shown in Figure 8, running processes in a sub-saturating regime can provide a viable tradeoff between throughput and precursor utilization.

V. CONCLUSIONS

In this work, we have explored the scalability of different strategies for particle coating by atomic layer deposition by analyzing the transition from reaction-limited to transport-limited regime. We have introduced four simple models encompassing both batch and continuous processes of particle coating with agitation. These models depend primarily on inputs available from either knowledge about the ALD process or the experimental conditions. They can help evaluate the scalability of different ALD processes and their implementation at manufacturing scale, something relevant for cost-sensitive applications such as catalysis, energy storage, and decarbonization. The models are available as part of the Python package `aldsim`. Specific models have also been released as a spreadsheet and made available in the GitHub

repository: <https://github.com/alddsim/alddsim>.

ACKNOWLEDGMENTS

This research is based upon work supported by Laboratory Directed Research and Development (LDRD) funding from Argonne National Laboratory, provided by the Director, Office of Science, of the U.S. Department of Energy under Contract No. DE-AC02-06CH11357. This work was supported in part by the Israel-U.S. Collaborative Water-Energy Research Center (CoWERC), supported by the Binational Industrial Research and Development Foundation under Energy Center grant EC-15.

DATA AVAILABILITY STATEMENT

The data that support the findings of this study are openly available in the GitHub repository: <https://github.com/alddsim/alddparticle>.

REFERENCES

- ¹D. Longrie, D. Deduytsche, and C. Detavernier, "Reactor concepts for atomic layer deposition on agitated particles: A review," *Journal of Vacuum Science & Technology A* **32**, 13 (2014).
- ²A. W. Weimer, "Particle atomic layer deposition," *Journal of Nanoparticle Research* **21**, 42 (2019).
- ³J. R. van Ommen and A. Goulas, "Atomic layer deposition on particulate materials," *Materials Today Chemistry* **14**, 9 (2019).
- ⁴Y. Koshtyal, D. Olkhovskii, A. Rumyantsev, and M. Maximov, "Applications and advantages of atomic layer deposition for lithium-ion batteries cathodes: Review," *Batteries-Basel* **8**, 41 (2022).
- ⁵K. Cao, J. M. Cai, X. Liu, and R. Chen, "Review article: Catalysts design and synthesis via selective atomic layer deposition," *Journal of Vacuum Science & Technology A* **36**, 12 (2018).
- ⁶Y. S. Jung, A. S. Cavanagh, A. C. Dillon, M. D. Groner, S. M. George, and S. H. Lee, "Enhanced stability of LiCoO₂ cathodes in lithium-ion batteries using surface modification by atomic layer deposition," *Journal of the Electrochemical Society* **157**, A75–A81 (2010).
- ⁷M. Lindblad, S. Haukka, A. Kytokivi, E. L. Lakomaa, A. Rautiainen, and T. Suntola, "Processing of catalysts by atomic layer epitaxy: modification of supports," *Applied Surface Science* **121**, 286–291 (1997).
- ⁸M. J. Pellin, P. C. Stair, G. Xiong, J. W. Elam, J. Birrell, L. Curtiss, S. M. George, C. Y. Han, L. Iton, H. Kung, M. Kung, and H. H. Wang, "Mesoporous catalytic membranes: Synthetic control of pore size and wall composition," *Catalysis Letters* **102**, 127–130 (2005).
- ⁹Y. Lei, B. Liu, J. Lu, R. J. Lobo-Lapidus, T. Wu, H. Feng, X. Xia, A. U. Mane, J. A. Libera, J. P. Greeley, J. T. Miller, and J. W. Elam, "Synthesis of Pt–Pd core–shell nanostructures by atomic layer deposition: Application in propane oxidative dehydrogenation to propylene," *Chemistry of Materials* **24**, 3525–3533 (2012).
- ¹⁰J. Lu, K.-B. Low, Y. Lei, J. A. Libera, A. Nicholls, P. C. Stair, and J. W. Elam, "Toward atomically-precise synthesis of supported bimetallic nanoparticles using atomic layer deposition," *Nature Communications* **5** (2014), 10.1038/ncomms4264.
- ¹¹H. Feng, J. L. Lu, P. C. Stair, and J. W. Elam, "Alumina over-coating on Pd nanoparticle catalysts by atomic layer deposition: Enhanced stability and reactivity," *Catalysis Letters* **141**, 512–517 (2011).
- ¹²J. L. Lu, B. S. Fu, M. C. Kung, G. M. Xiao, J. W. Elam, H. H. Kung, and P. C. Stair, "Coking- and sintering-resistant palladium catalysts achieved through atomic layer deposition," *Science* **335**, 1205–1208 (2012).
- ¹³J. A. McCormick, B. L. Cloutier, A. W. Weimer, and S. M. George, "Rotary reactor for atomic layer deposition on large quantities of nanoparticles," *Journal of Vacuum Science & Technology A* **25**, 67–74 (2007).
- ¹⁴M. W. Coile, M. J. Young, J. A. Libera, A. U. Mane, and J. W. Elam, "High-capacity rotary drum for atomic layer deposition onto powders and small mechanical parts in a hot-walled viscous flow reactor," *Journal of Vacuum Science & Technology A* **38**, 10 (2020).
- ¹⁵L. F. Hakim, J. A. McCormick, G. D. Zhan, A. W. Weimer, P. Li, and S. M. George, "Surface modification of titania nanoparticles using ultrathin ceramic films," *Journal of the American Ceramic Society* **89**, 3070–3075 (2006).
- ¹⁶J. R. van Ommen, D. Kooijman, M. de Niet, M. Talebi, and A. Goulas, "Continuous production of nanostructured particles using spatial atomic layer deposition," *Journal of Vacuum Science & Technology A* **33**, 5 (2015).
- ¹⁷J. Hartig, H. C. Howard, T. J. Stelmach, and A. W. Weimer, "DEM modeling of fine powder convection in a continuous vibrating bed reactor," *Powder Technology* **386**, 209–220 (2021).
- ¹⁸A. Yanguas-Gil and J. W. Elam, "Self-limited reaction-diffusion in nanostructured substrates: Surface coverage dynamics and analytic approximations to ald saturation times," *Chemical Vapor Deposition* **18**, 46–52 (2012).
- ¹⁹Z. Lu, A. Yanguas-Gil, D. H. Y. Kang, P. Darapaneni, A. U. Mane, C. L. Marshall, and J. W. Elam, "Scalable synthesis of supported catalysts using fluidized bed atomic layer deposition," *Journal of Vacuum Science & Technology A* **40**, 12 (2022).
- ²⁰R. J. Kee, M. E. Coltrin, P. Glarborg, and H. Zhu, *Chemically reacting flow : theory, modeling, and simulation*, second edition. ed. (John Wiley & Sons, Hoboken, NJ, USA, 2018) pp. xli, 747 pages.
- ²¹J. Dendooven, D. Deduytsche, J. Musschoot, R. L. Vanmeirhaeghe, and C. Detavernier, "Modeling the conformality of atomic layer deposition: The effect of sticking probability," *Journal of the Electrochemical Society* **156**, P63–P67 (2009).
- ²²A. Yanguas-Gil and J. W. Elam, "Simple model for atomic layer deposition precursor reaction and transport in a viscous-flow tubular reactor," *Journal of Vacuum Science & Technology A* **30** (2012), 10.1116/1.3670396.
- ²³K. Arts, M. Utriainen, R. L. Puurunen, W. M. M. Kessels, and H. C. M. Knoops, "Film conformality and extracted recombination probabilities of o atoms during plasma-assisted atomic layer deposition of SiO₂, TiO₂, Al₂O₃, and HfO₂," *Journal of Physical Chemistry C* **123**, 27030–27035 (2019).
- ²⁴A. Yanguas-Gil, J. A. Libera, and J. W. Elam, "Reactor scale simulations of ald and ale: Ideal and non-ideal self-limited processes in a cylindrical and a 300 mm wafer cross-flow reactor," *Journal of Vacuum Science & Technology A* **39** (2021), 10.1116/6.0001212.
- ²⁵A. R. Bielinski, E. P. Kamphaus, L. Cheng, and A. B. F. Martinson, "Resolving the heat of trimethylaluminum and water atomic layer deposition half-reactions," *Journal of the American Chemical Society* **144**, 15203–15210 (2022).
- ²⁶J. Hartig, V. Dahanayake, J. Nguyen, C. Wilson, A. M. Barnes, and A. W. Weimer, "A moving porous media model for continuous spatial particle ALD," *Powder Technology* **421** (2023), 10.1016/j.powtec.2023.118448.